JOURNAL OF MATERIALS SCIENCE 30 (1995) 2968–2980

Fractal and topological characterization of branching patterns on the fracture surface of cross-linked dimethacrylate resins

Part I

Z. V. DJORDJEVIC, X. FENG LI, WON SOO SHIN, S. L. WUNDER*, G. R. BARAN[1]
Department of Chemistry, Temple University, Philadelphia, PA 19122, and
[1]*School of Dentistry, Temple University, Philadelphia, PA 19140, USA*

The branching patterns formed as a result of crack growth in dimethacrylate resins below their glass transition temperatures looked similar to fractal trees. The skeletons of the patterns were analysed numerically for their topological and geometrical properties. The number of branches, N_i, mean branch lengths, L_i, and branch angles of a particular order, defined according to the Strahler and inverted Weibel schemes, followed exponential scaling behaviour: $N_i \sim (R_B)^{-i}$ and $L_i \sim (R_L)^i$. Using the relationship for the fractal dimension $D = \ln R_B / \ln R_L$, a value of $D = 1.4$ was obtained for the fracture pattern. Fractal behaviour was also examined by the box-counting method which indicated a power-law dependence of the mass on the box size with fractal dimension exponent $D = 1.4$ in the case of the fracture pattern. However, the mass–shell method for both the fracture pattern and the fractal trees gave an exponential increase of mass with distance from the origin, rather than the power-law behaviour expected for fractals. This was attributed to the fact that branches of different sizes were distributed in restricted regions of space closer to the periphery, rather than uniformly over the whole pattern.

1. Introduction

It has long been known that materials that fracture in a nominally brittle manner exhibit plastic deformation at the crack tip and do not behave as ideal elastic brittle solids [1]. Fracture in these materials produces a wide range of surface morphologies. Patterns, such as regular arrays of parallel lines and branching patterns, in the crack plane, have been observed in thermoset resins (phenol-formaldehyde, unsaturated polyesters, cross-linked polymethylmethacrylate, epoxide resins, polyethylene glycol dimethacrylate doped with polymethylmethacrylate) and in uncross-linked polymers (polymethylmethacrylate, low-density polyethylene) fractured using a variety of loading conditions [2–4]. These features have been referred to as "river markings", "finger-like furrows", "striations" and "welts". Tree-like patterns have also been observed in the fracture surfaces of metallic glasses and brittle solids such as crystals of Cu_2Mg [5, 6].

Many other naturally occurring patterns, such as river networks, vascular systems, lungs etc., have tree-like structure and these have been described by various ordering schemes [7–10] for which exponential scaling behaviour of relevant branch properties (such as length, width and number of branches) has been observed. This implies that the ratios between properties for subsequent branch orders (the bifurcation or length ratios) are constant. Recently, diffusion-limited clusters and viscous fingering patterns have also been characterized using ordering schemes for their branches [11–13], and it was found here too that branch properties (number, mass, length and width) depended exponentially on branch order.

A recent approach to the understanding of fracture phenomena is the fractal characterization [14–16] of the morphologies of fracture surfaces. This method provides a quantitative, systematic approach to the characterization of complex disordered structures. For these systems, the dependence of an appropriate measure (mass, area, etc.) on linear dimension can be described by a power-law dependence with a non-integer fractal dimension exponent, D, which is smaller than the Euclidean dimension of the structure. Computer models using Monte Carlo methods [17, 18] have been used to reproduce these characteristic fracture patterns. DLA [19] is the leading model of fractal growth [15, 16, 20] and many two-dimensional growth processes exhibit regimes in which the observed patterns resemble DLA clusters with $D \approx 1.7$ [20]. A modified DLA model [21, 22] has been used

* Author to whom all correspondence should be addressed.

0022–2461

to describe dielectric breakdown and viscous fingering (fluid–fluid displacement), phenomena which can be considered to be primitive model systems for fracture. Viscous fingering patterns (in model systems) have been shown to exhibit behaviour ranging from that typical of DLA at low pressure to that of non-fractal dense branching morphologies at higher pressures [23, 24].

In very general terms, fractals are structures or shapes that have the same degree of complexity on different length scales; i.e. the structures appear self-similar under different magnifications. The most simple types of fractals, homogeneous self-similar fractals, are those invariant to an isotropic change of length scales. In some other cases, the fractal structure is invarient to an "affine" transformation [14–16, 25, 26] in which the length scale is changed by different factors in different directions. Many objects in nature can be represented by random fractals that are self-similar or self-affine structures in a statistical sense; their geometrical properties and distribution functions exhibit scaling laws on different length scales only when averaged over many samples. Deterministic fractals, such as Koch curves, Cantor sets and Sierpinski gaskets, are obtained by defining a mathematical initiator and generator from which the self-similar fractal structure is generated. Similarly, fractal trees can be formed by specific rules, forming a class of deterministic, self-similar, non-uniform fractals [14, 27]. These trees have relevance for the present work because of the similarity in appearance between these structures and the patterns obtained from the fracture surfaces.

It was the purpose of this work to characterize quantitatively the branched structures produced in the fracture surface of a highly cross-linked ethoxylated bisphenol A dimethacrylate resin, in the hope that the statistical characteristics of the patterns may eventually provide insight on the failure mechanisms in brittle materials. In particular, the topological, geometrical and fractal properties of the two-dimensional fracture patterns have been characterized using scaling concepts and fractal geometry. These patterns will be compared with fractal trees formed according to well-defined growth rules for which scaling behaviour of relevant branch properties is established by definition [14].

2. Experimental procedure

2.1. Materials

Samples of ethoxylated bisphenol-A dimethacrylate (EBPADMA) monomer (ESSCHEM Co.) inhibited with 100 p.p.m. hydroquinone, were heat cured using 1% benzoyl peroxide (Aldrich Chemicals) as initiator. The degree of conversion was determined to be 90% by Fourier transform–Raman spectroscopy [28]. The sample was below its glass transition temperature, determined to be 123 °C using the loss modulus curve and 180 °C using the tan δ peak from dynamic mechanical analysis. Samples to be fractured were cut with a diamond saw from the original cylindrical shape into discs 5 mm thick and 6 mm diameter.

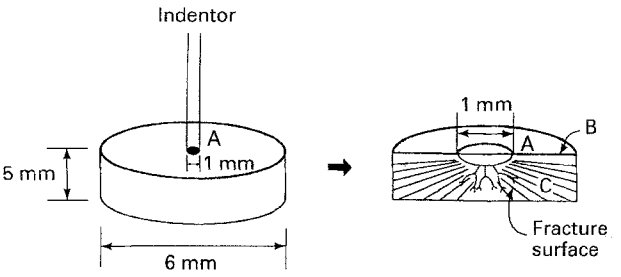

Figure 1 Schematic drawing of the loading geometry and the fractured specimen. A 1 mm spherical indentor is applied to surface A to produce the fractured specimen. The fracture surface, C, contains the characteristic branched structures and nearly parallel striations. The edge between the perpendicular surfaces A and C is marked B and these labels are used in order to help identify these regions in the real fracture pattern.

2.2. Specimen preparation and fractography

The ethoxylatedbisphenol-A dimethacrylate resins were fractured using a 1 mm indentor. An MTS mechanical tester operating at 50 Hz, i.e. at a speed of 38 mm s^{-1} was used to apply a load to the sample sufficient to cause "brittle" failure. Typical loads were 381–445 N. A schematic illustration of the fracture produced by this loading mechanism is shown in Fig. 1, where the load-bearing surface is labelled A, the fracture surface is labelled C and the intersection of these two perpendicular surfaces is the line labelled B. The sample was first loaded in compression and failed in Mode 1 tension. The fracture surfaces were gold coated and observed in a scanning electron microscope.

2.3. Digitization

The patterns were digitized using a high-resolution video frame grabber (v.f.g.) interfaced to a PC/AT microcomputer. The video camera was a Panasonic WV1500A480 line black and white videcon, with a photographic stand and back illumination capability. The v.f.g. digitized images to 480 by 512 pixels with 8 bits of resolution. Processing software, written in machine assembly language, with standard routines for digital image manipulation such as contrast enhancement, panning and zooming was used. The digital images were interactively analysed using a pointing device, which had the capacity to either define a coordinate or assign a label. A discrete set of points was used to describe each branch of the skeleton. The density of points was determined by the curvature of the particular section of the branch: straighter portions of the branch needed fewer points than curved portions. The skeleton formed in this manner was overlaid on the real image so that decisions concerning exact locations of branching points and branch tips were made by the operator.

The data obtained in this way was transferred in plain text files to either an IBM Risk 6000 or IBM 486 PC to be analysed further. The branches were relabelled to contain information on the generation order, number of branches in a particular generation and the parent branch labelling. A Fortran program was applied to connect the data points into a branching

structure which corresponded to the original skeleton. Any pixels through which these lines passed were considered to be occupied.

3. Results

3.1. Qualitative characterization of the fracture surface

A typical surface is shown in Fig. 2a, at low magnification. The overview is labelled in the same way as the schematic drawing and includes the region near the spherical tip of the indentor, "a", followed by the furrowed "river" region, from "b" to "c", covering roughly 0.5 mm and lastly by the smooth or "mirror" region, "d". The "river" region, a portion of which is shown at higher magnification in Fig. 2b, contains the morphology described by Robertson and Mindroiu [29] as "steps" and "welts" (middle of figure) and the "stacked lamellar texture" (top of figure). The smooth region shown both in Fig. 2b and at higher

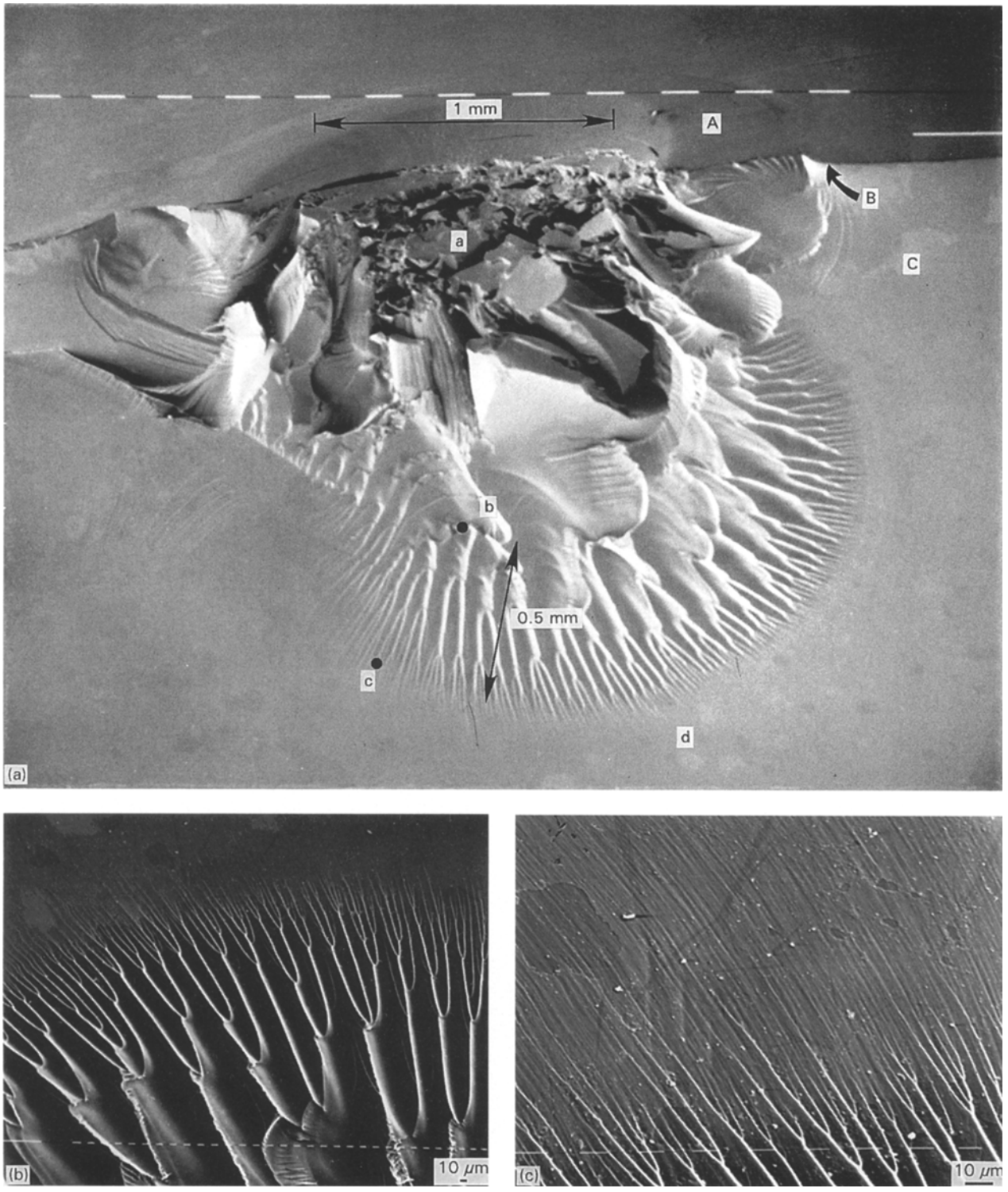

Figure 2 (a) Low-magnification electron micrograph of fracture surface. A, C and B indicate the top surface, fracture surface and intersection of these two surfaces, respectively, as shown schematically in Fig. 1. The region damaged by the spherical indentor before fracture is marked "a". The circular region from "b" to "c" is the furrowed "river" region. The mirror region is marked "d" and at higher magnifications shows nearly parallel densely spaced striations, shown in Fig. 4. (b) Higher magnification electron micrograph of fracture surface C in the circular region between "b" and "c", showing branched "river markings". (c) Highest magnification electron micrograph of fracture surface C, at the end of the circular region from "b" to "c", and the beginning of region "d", showing the nearly parallel densely spaced striations.

magnification in Fig. 2c actually contains striations described by Robertson and co-workers [29–31] as the "basic longitudinal texture". This figure shows more clearly the branched structures tapering off into the nearly parallel striations and demonstrates the difficulties in determining the ends of the branch tips.

The region of increased complexity, shown in Fig. 2a from "b" to "c" and at higher magnification in Fig. 2b, can also be observed using an optical microscope. When viewed directly (i.e. in a backscattering geometry) under the light microscope it is apparent that the dark regions are not "furrows", but instead are steps connecting two surfaces on different planes. This has been confirmed using confocal microscopy.

The pattern as a whole exhibits radial symmetry, as can be seen in Fig. 2a, with the branch tips ending in a circular envelope around the indentation area. There are at least 25 separate major branches which originate in a region below that damaged by the indentor. The branch segments exhibit curvature toward the radial direction, which allows them avoid each other as they further propagate and branch. This allows a greater number of generations to occur than if the branches followed straight lines in the initial growth direction. Binary branching (two branches emanating from a branching point) is dominant with occasional occurrence of ternary branching. Terminal branches can occasionally be seen emanating close to the origin. Qualitatively, it can be seen that the empty space between branches closer to the initial indentation is larger than in the region where the pattern terminates. On average, the branches closest to the tips are shorter than those closer to the initial branch and the angles (although curved) formed by the branch tips are smaller than those formed at the primary branches.

The fracture pattern in Fig. 2a–c shows that portions of the pattern observed at high magnification are similar to the whole pattern observed at low magnification. In addition, patterns formed in the same material which are observable to the naked eye also have a similar appearance. This indicates that some ordering principle may be involved in the pattern formation and that the patterns may exhibit some aspects of self-similarity or self-afinity (scale invariance) [14–16]. The patterns can be described as trees in the sense that branching occurs with self-avoidance of the branch segments, i.e. there are no closed loops.

3.2. Quantitative characterization of branching patterns: topological and geometrical properties

The patterns have been analysed for two-dimensional length and angle information defined by the skeleton. The word "skeleton" is used for the graph created by the centre lines of all branches of the fracture pattern. The intersection of two branch segments is called a node or branching point. The topological properties [14] of a branching structure, which reflect connectivity properties unaffected by changes in lengths or angles of the branches, are retained if this structure is treated as a tree in a mathematical sense, i.e. as a set of connected nodes without loops, and can be studied using combinatorial concepts [32]. Geometrical properties [14] such as distributions of branch lengths, diameters of branches, branching angles and curvature, provide complementary information. The spatial distribution of the measure of a branching structure can be characterized using concepts from fractal geometry [14–16], providing an additional geometrical characterization of the pattern.

3.2.1. Ordering schemes

In order to characterize a branched structure, it is convenient to define an ordering scheme for its segments. Hydrogeologists were the first to propose such ordering schemes for river networks [7–9] and these schemes were subsequently accepted in many other areas in which branching structures are relevant, such as biology [33, 34] (brain cells [35], blood vessels [36, 37], lungs [33, 34], etc.) and fracture [4]. Two particular schemes, namely the Weibel [10, 33] and Strahler schemes [8, 9, 33] are the most commonly employed in the characterization of branching structures and we found them very useful for characterizing the fracture patterns considered in this work.

In the case of Strahler scheme, presented in Fig. 3a, any branch ending with no side branches is designated order 1 and when two first-order branches meet, they form a branch of order 2. The rules used to designate order are that when two branches of the same order meet they form a branch of one higher order, and when branches of different order meet, the order of the conjoined branch remains that of the branch of highest order. In Weibel's scheme, Fig. 3b, the order of successive bifurcations of a branching structure is labelled by the "generation" or "shell" number. The trunk (branch segment closest to the origin) is designated order 1. The order of subsequent branch segments is increased by 1 at each node going away from the origin. If the last segments (tips) of each major branch, which are of highest order according to the Weibel scheme, are redefined to be the lowest order branches, i.e. of order 1, and similarly branches that were one order smaller than the maximum order become of order 2 and so on until the trunk is reached, one obtains the inverted Weibel scheme, shown in Fig. 3c. A tree ordered by the Strahler scheme will have fewer branches and smaller order than the same tree ordered by the Weibel scheme, because the Strahler order increases only when two branches of the same order meet. Because the "tips" of the branches of the pattern ended in a well-defined arrest line, whereas the "trunks" or "roots" originated in the damage region which did not have a well-defined origin, the Strahler and inverted Weibel schemes, where the first order branches were the tips, were more appropriate for the analysis of our fracture patterns.

The fracture patterns exhibited curvature of the branches, so the branch segments and angles were either described in terms of a skeleton with linear segments between the nodes or a skeleton in which branch segments truly followed the actual pattern, as shown in Fig. 4. The former will be referred to as a "stick" model and the latter as a "curved" model.

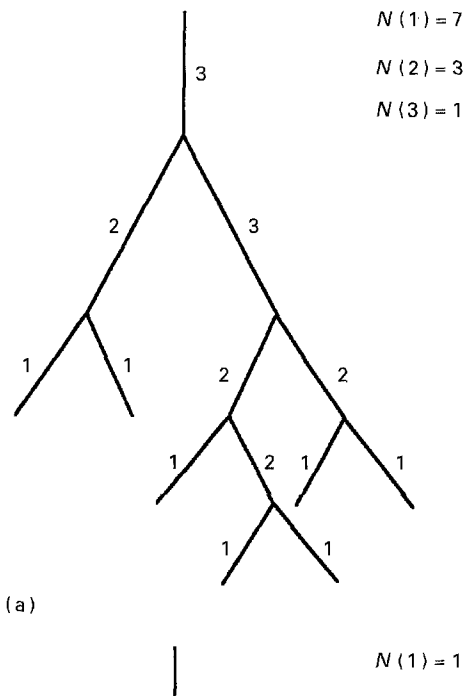

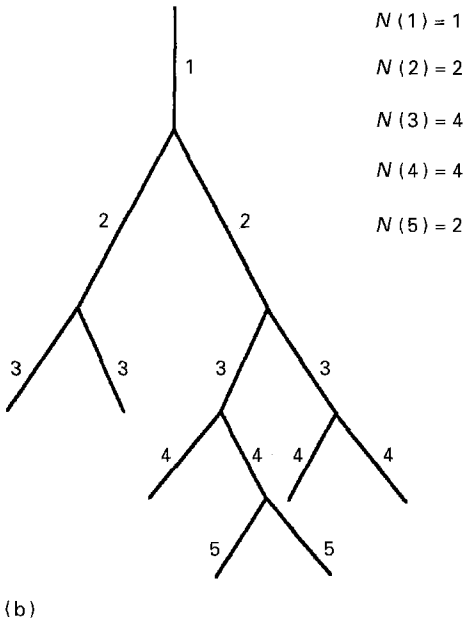

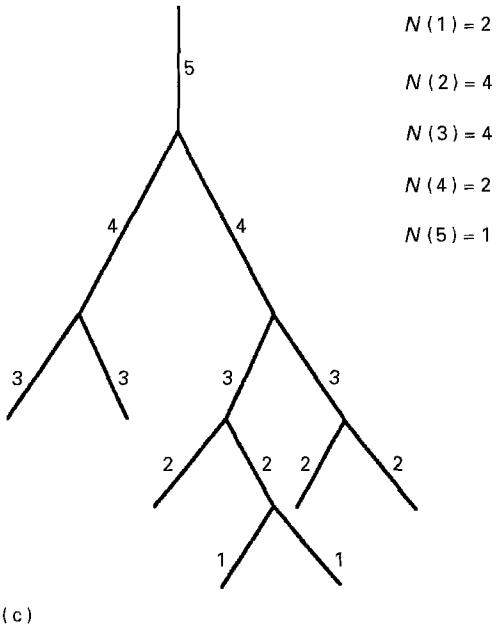

Figure 3 Schematic drawings of (a) an asymmetrical branched structure labelled according to the Strahler scheme, (b) the same branched structure labelled according to the Weibel scheme, and (c) the same branched structure labelled according to the inverted Weibel scheme.

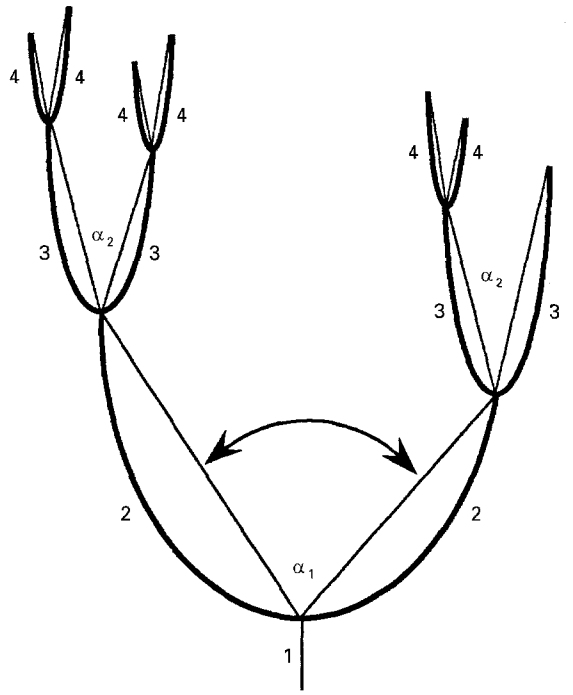

Figure 4 Schematic drawing of the (——) "stick" and (——) "curved" models of the fracture pattern according to the Weibel ordering scheme.

For the "stick" model the branch angles are well defined and the order of the branch angle is designated the order of the "parental" branch from which the sides of the angle emanate, as shown in Fig. 4 for the case of the Weibel scheme.

Our aim in this part of the work was to determine if topological as well as geometrical properties of the fracture pattern could be described by simple scaling laws in terms of branch order, as has been done in the case of river networks and lungs. For this purpose, we counted the number of branches in each order for each major branch and determined their mean lengths for both the stick and curved skeleton models, using the Strahler, Weibel and inverted Weibel schemes. Branch angles were counted and measured as a function of branch order from the stick skeleton, but only using the Weibel and inverted Weibel schemes. The whole pattern was then characterized by superimposing and averaging the properties of the individual major branches.

3.2.2. Number of branches and branch-length distribution

Using Strahler's ordering scheme and either the "curved" or "stick" skeleton, we found that the number of branches, N_i, of order i obeyed an exponential law

$$N_i \sim (R_B)^{-i} \tag{1a}$$

where R_B is the branching (bifurcation) ratio, defined in the asymptotic region as

$$R_B = N_i / N_{i+1} \tag{1b}$$

The number of branches, N_i, in successive orders decreases by a constant factor equal to the branching ratio, R_B. The branching ratio is obtained from the

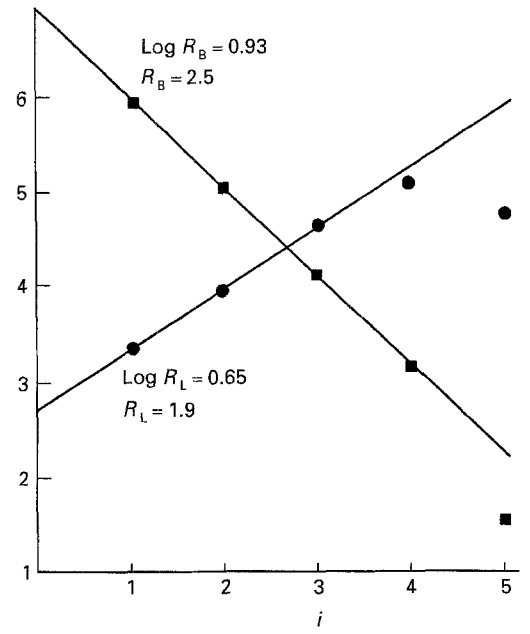

Figure 5 Dependence Weibel ordering scheme log N_i and log L_i on the order i. (■) N_i, the number of branches of order i; (●) L_i, the average length of branches of order i.

slope of the log N_i versus order i plot. Similar relationships were found for the mean lengths of branches of order i

$$L_i \sim (R_L)^i \tag{2a}$$

where R_L is the branch length ratio defined as

$$R_L = L_{i+1}/L_i. \tag{2b}$$

The log of the number N_i of branches of order i is plotted versus order i in Fig. 5 for the case of the Strahler ordering scheme for the "curved" skeleton. These data can be represented quite well by a straight line with four orders out of the maximum of five observed in the patterns falling near the line. Here, order 1 corresponds to the tips and order 5 corresponds to the roots; it is more difficult to obtain good data near the damage region of the sample where the roots begin. According to Equation 1a, the slope of this line in the asymptotic region of small orders gives the value of $\ln(R_B) = 0.93 \pm 0.02$, and a bifurcation ratio $R_B = 2.5 \pm 0.05$. These data, along with data obtained for the "stick" model are presented in Table I, where the values of R_B obtained are within the experimental uncertainty.

It can be shown that in the case of the Strahler ordering scheme the branching ratio R_B, has a lower limit of 2 in the case of symmetrical binary trees, defined as ones in which branches bifurcate at each node on the shell. For asymmetrical trees, for which bifurcation at each node does not necessarily occur, the values of R_B greater than 2 are expected, with increasing values characterizing increasing degrees of asymmetry of the tree pattern. In the limit of a completely asymmetrical tree, which corresponds to comb structures, the branching ratio, R_B, is equal to the number of side branches, b [32, 38], which can be an arbitrarily large number. The value of $R_B = 2.5$ found for the fracture patterns is thus close to the value $R_B = 2$ for symmetrical trees. It should be noted that the closer the tree pattern is to a symmetrical one, the more the order of the tree and R_B are affected by the loss (removal) of branch segments, especially the tips. This can occur, for example, if the branch tips are not considered due to lack of resolution in the electron microscope picture or in the digitized image.

TABLE I Values of the bifurcation ratio, R_B, length ratio, R_L, and fractal dimension, D, $D = \log(R_B)/\log(R_L)$, for the curved and stick skeleton in the case of Strahler and inverted Weibel schemes

Scheme	Skeleton type	Dependence	R_B	R_L	D
Strahler	Curved	Exponential	2.5	1.9	1.43
	Stick	Exponential	2.5	1.9	1.43
Inverted	Curved	Exponential	1.8	1.6	1.3
Weibel	Stick	Exponential	1.8	1.5	1.4

The logarithm of the mean length, L_i, for all branches of order i is also plotted versus i in Fig. 5 for the case of the "curved" skeleton. From the slope of the straight line drawn through the data, $\log(R_L) = 0.65 \pm 0.05$ and thus $R_L = 1.9 \pm 0.1$. These results, along with those for the "stick" model, are summarized in Table I; it can be seen that both curved and stick models yield similar values of R_L.

When the inverted Weibel ordering scheme is used with either the "stick" skeleton or "curved" skeleton description of the branching pattern, N_i and L_i also exhibited an exponential dependence on i as in Equation 1a and b, with $\log(R_B) = 0.6 \pm 0.03$ ($R_B = 1.8$) and $\log(R_L) = 0.4 \pm 0.05$ ($R_L = 1.5$) for the stick skeleton and $\log(R_B) = 0.6 \pm 0.03$ ($R_B = 1.8$) and $\log(R_L) = 0.45 \pm 0.05$ ($R_L = 1.6$) for the curved skeleton. These data are also presented in Table I. However, only 3 or 4 orders (out of a maximum order of 7) could be fit by a straight line on the semi-log plot. In the case of the inverted Weibel scheme the branching ratio, R_B, has an upper limit of 2 in the case of a symmetrical binary tree and for asymmetrical trees, values of R_B less than 2 are expected, with decreasing values characterizing increasing degrees of asymmetry of the tree pattern. For a completely asymmetrical tree (i.e. a linear comb with b teeth) the value of R_B is equal to 1 [39]. Thus, the values obtained for the fracture patterns using the inverted Weibel scheme also indicate that the fracture pattern was closer to a symmetrical one.

When Weibel's ordering scheme and either a stick skeleton or a curved skeleton was used, the dependence of N_i and L_i on order i was better fit using a power law rather than an exponential.

3.2.3. Distribution of branch angles

It is apparent from Fig. 2a–c that the average angle decreases from that observed at the root of the branching structure to that observed at the tips. Because the average branching angle decreases with generation number from the root of the skeleton, the structure (angles) close to the root, for example, cannot be obtained from those close to the tips by

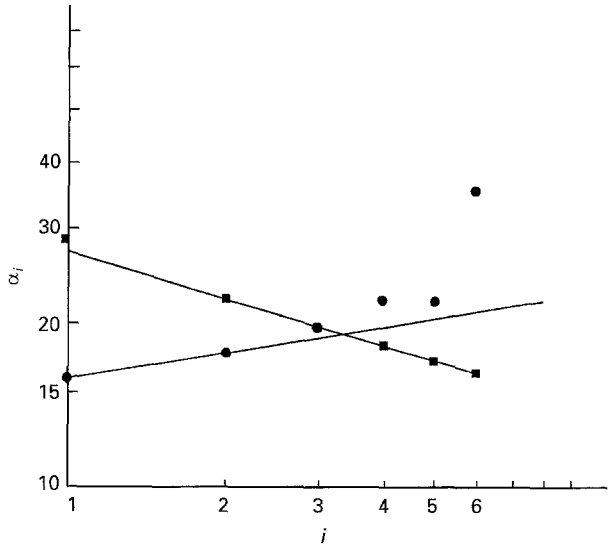

Figure 6 Dependence of log α_i on log i, where α_i is the average branch angle and i is ordered according to the (■) Weibel and (●) inverted Weibel schemes.

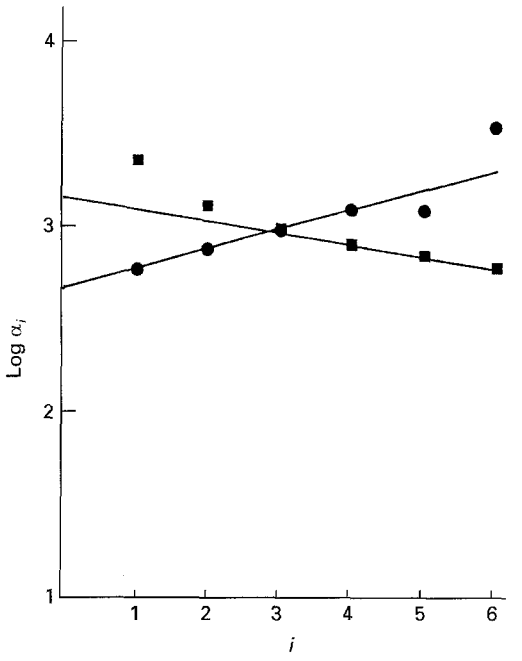

Figure 7 Dependence of log α_i on order i, where α_i is the average branch angle and i is ordered according to the (■) Weibel and (●) inverted Weibel schemes.

applying the same scale transformation in both the radial and tangential directions.

In order to find the dependence of the angle on branching order, it is more convenient to apply the Weibel and inverted Weibel schemes, with angles defined according to the "stick" skeleton model, in which the nodes of the skeleton are connected by straight lines to parental nodes, as illustrated in Fig. 4. The dependence of the log of the average branch angle, α_i, on log i, in the case of both Weibel and inverted Weibel scheme, is presented in Fig. 6. The good linear fit (for 5 out of 6 orders) observed in the case of the Weibel scheme implies a power law dependence of α_i on i, i.e.

$$\alpha_i \sim i^x \tag{4a}$$

A value of $x = 0.3$ was obtained from the slope of the log–log plot in the asymptotic, large i region. When the pattern is ordered according to the inverted Weibel scheme, linear behaviour is observed on a plot of $\log(\alpha_i)$ versus i, shown in Fig. 7, implying that in that case the dependence of α_i on i is exponential, i.e.

$$\alpha_i \sim (R_\alpha)^{-i} \tag{4b}$$

A value of $\ln(R_\alpha) = 0.12$ is obtained from the slope of the plot, giving $R_\alpha = 1.13$. For the range of angles observed in our patterns, this scaling behaviour indicates that the angles change as a power law from a value of 30° near the roots to a value of 16° at the tips for the Weibel ordering system, and exponentially from 35° near the roots to a value of 16° at the tips for the inverted Weibel scheme.

3.3. Fractal analysis

A fractal is an object which has the same degree of complexity on all length scales. In the most simple case of homogeneous fractals, it is possible to scale one part of the structure to another by an isotropic change of length scale. A homogeneous self-similar fractal can thus be characterized in a simple way by its fractal dimension, D, which expresses how the average "mass" $\langle M(R) \rangle$ within a circle of radius, R (centred on an occupied part of the fractal) scales with R [15–18], i.e.

$$\langle M(R) \rangle \sim R^D \tag{5}$$

For Euclidean objects in one dimension, $D = 1$ and in two dimensions, $D = 2$. In the case of fractal objects in two dimensions $1 \leqslant D \leqslant 2$.

Another approach commonly used to determine the fractal dimension D of a fractal structure is the box-counting method [16–18], where a grid of boxes of linear dimension, ε, is placed on the pattern and the number of boxes fully or partially filled by the pattern is counted (the smallest size of ε is typically the size of a pixel in a digitized image and is increased until ε is of the order of the size of the whole pattern). A homogeneous, self-similar fractal number of boxes covered by the pattern scales as

$$M(\varepsilon) \sim \varepsilon^{-D} \tag{6}$$

By plotting $\log[M(\varepsilon)]$ versus $\log \varepsilon$ for different values of ε, the fractal dimension D can be obtained from the slope of the graph. We have used a new variable k defined in terms of ε as $\varepsilon = 2^{k-1}$. It corresponds to increasing the linear size of the boxes by a factor of 2 at each iteration k; i.e. $k = 1$ corresponds to boxes of size one pixel, $k = 2$ corresponds to boxes of size 2 pixels, $k = 3$ corresponds to boxes of size 2^2 pixels, etc. The fractal dimension, D, can be deduced from the slope of the plot of $\log[M(k)]/\log 2$ versus k (because $\varepsilon = 2^{k-1}$), shown in Fig. 8. The plot can be separated into two linear regions. For small values of k (up to $k = 3$), corresponding to high resolution (i.e. smaller length scales), the slope of the plot gives a fractal dimension $D = 0.9$ which is close to the expected value

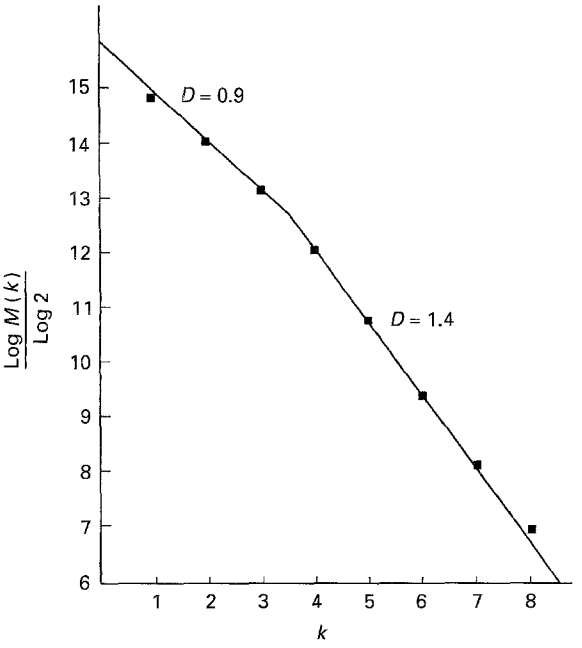

Figure 8 Plot of log $[M(k)]$/log 2 versus k, where $\varepsilon = 2^{k-1}$, showing two scaling regimes. At small k, or higher resolution, the slope is $D = 0.9$ and at large k or lower resolution, $D = 1.4$.

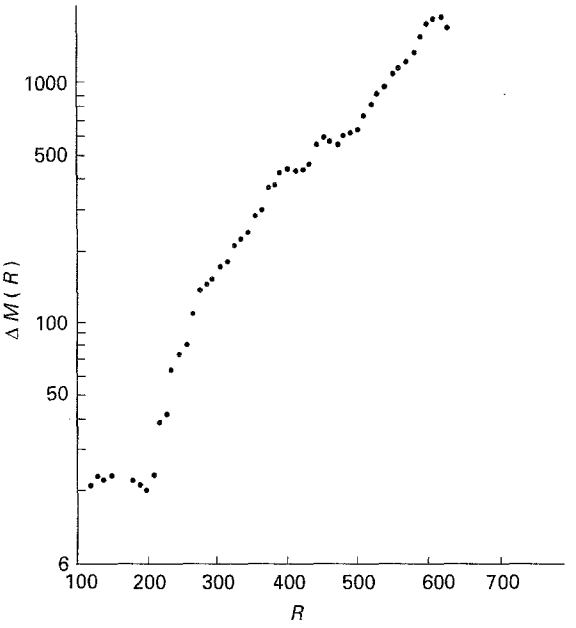

Figure 9 Semilog plot of the shell mass, ΔM, versus, R, for fracture pattern. R is measured in units of pixels and ΔR corresponding to $\Delta M(R)$ had a constant value of 10 pixels.

$D = 1$. For larger values of $k (k > 3)$, corresponding to lower resolution (i.e. larger length scales), the data fall on a straight line of slope, $D = 1.4 \pm 0.1$. The value of k at which the crossover occurs is called k_{cr}. It is only for values of k larger than the crossover value that the fractal geometry of the pattern is observed.

For fractal branching structures with branching ratio, R_B, and length ratio, R_L, the fractal dimension exponent, D, can also be expressed as [15, 39]

$$D = \log(R_B)/\log(R_L) \quad (7)$$

Values of D obtained using this relation for the case of the Strahler and inverted Weibel and ordering schemes are presented in Table I. Equation 7 was derived for the case of exponential dependences of N_i and L_i on the branching order i. We observed the exponential relations only when the Strahler and inverted Weibel schemes were used to characterize the fracture pattern. For the Strahler scheme, $\log(R_B) = 0.93$ and $\log(R_L) = 0.65$, so that $D = 1.43$ and for the inverted Weibel scheme $\log(R_B) = 0.6$ and $\log(R_L) = 0.45$ implying that $D = 1.3$. These values of D are in good agreement with the value of $D = 1.4$ obtained using the box counting method.

A variant on the mass radius method for determining the fractal dimension, D, is to take the derivative of Equation 5, giving $\Delta M/\Delta R \sim R^{D-1}$. The concentric geometry of our pattern makes the use of this mass–shell method for determining the fractal dimension appropriate. In this method, a sequence of concentric shells of radius R and width ΔR (we chose $\Delta R = 10$ pixels, and R in the range (100, 650)) is constructed about an appropriately chosen origin, corresponding to the origin of the fracture pattern. Therefore, the mass, ΔM, of a fractal object within shells of increasing distance from the origin should scale as

$$\Delta M \sim R^{D-1} \Delta R \quad (8)$$

By plotting ΔM versus R on a log–log graph, the value of the fractal dimension $(D - 1)$ can be obtained from the slope. In our case, the data plotted in this way are not linear. Instead, a semilog plot of ΔM versus R, shown in Fig. 9, is linear over a finite range of R values; i.e. between the lower and upper cut-off lengths determined by the indentation region and size of the pattern, respectively. This result clearly indicates that there is an exponential increase of shell *mass* with increasing shell radius ($\Delta M \sim e^{cR} \Delta R$) where c is a constant. This dependence also implies that the mass density is increasing as we go further from the centre of the pattern. For the fracture pattern shown in Fig. 2a–c, it can be seen that the branches are closer together at each level, packing space more densely further from the origin.

3.4. Fractal trees

The fracture patterns resemble trees with branching ratios equal to approximately 2 and with a distribution of branch lengths at each level (generation). The number of generations observed for the patterns is relatively small (less than 8). In order to understand the crossover behaviour and finite size effects that occur in real systems, and how these affect scaling behaviour and values of the fractal dimension obtained, we have performed numerical analyses on fractal symmetrical binary trees ($R_B = 2$) defined by Mandelbrot [14]. The trees are deterministic structures formed by infinitely thin stems in which the branching ratio, R_B, equals 2 and the length ratio, R_L, is constant; i.e. in each generation all the segments are

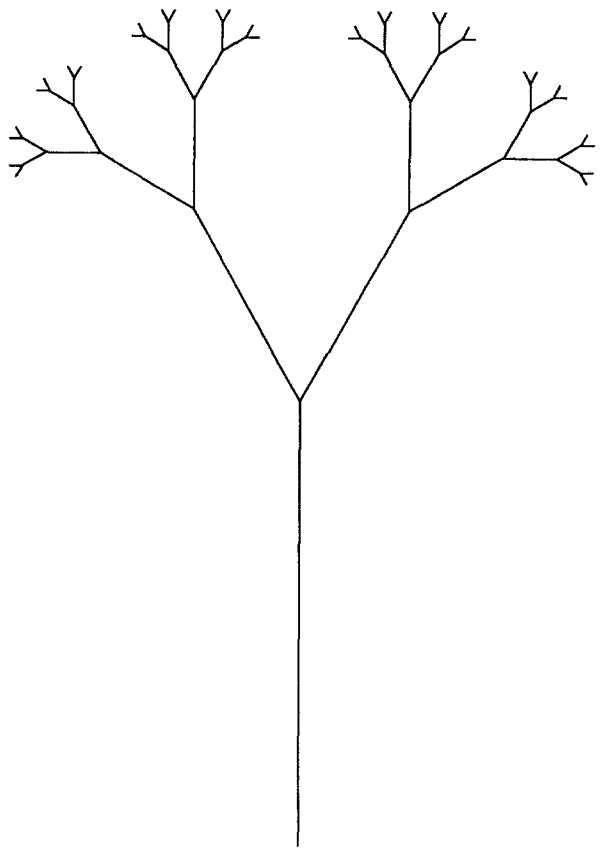

Figure 10 An example of an exact tree with $R_L = 2$ and $\theta = \pi/6$.

of the same length and the interbranch angle takes the same values at every node. An example of a fractal tree with $R_L = 2$ and $\theta = \pi/6$ is shown in Fig. 10. We have analysed fractal trees with varying length ratios, R_L, and branching angles, θ, as a function of number of generations and resolution. Further, we developed a model in which the angle for successive generations decreased as a power law with increasing generation order.

For fractal trees [14, 27] the fractal dimension changes for different parts of the structure. The stems, in the interior of the structure, are one-dimensional ($D = 1$) and the tips have a different fractal dimension ($1 < D \leqslant 2$) for a tree embedded in two-dimensional Euclidean space. Mandelbrot called these exact trees non-uniform fractals owing to the fact that their fractal dimension, D, takes different values for different parts of the structure. The whole tree has fractal dimension equal to D (where D is the larger of the two values of 1 or $D = \log 2/\log (R_L)$), because the larger fractal dimension dominates the overall scaling behaviour. In order to obtain values of D between 1 and 2 (which span the range of our real fracture patterns), R_L must lie between $2^{1/2}$ and 2 due to relation $D = \log 2/\log (R_L)$. The fractal dimension of the tree does not depend on the branching angle as long as self-avoidance (i.e. the branches do not cross each other) is fulfilled, although the shapes generated for various θ values look different (see, for example, Plate 155 in [14]). For each R_L value there is a critical value, θ_{cr}, of the interbranch angle, θ, above which branches will intersect. It satisfies the relation

$$R_L \sin(\theta/2) - \sum_{i}^{g-2} \sin(i\theta/2)/R_L^i > 0 \qquad (9)$$

which is derived by requiring that any path of a fractal tree of length ratio R_L and branching angle θ, with initial branch in the x direction and the second order branch emanating at an angle $\theta/2$ with respect to the x-axis, does not intersect that axis and subsequently its image path, after an arbitrary number of generations, g.

We have applied the mass–shell and box-counting methods numerically to Mandelbrot's fractal binary trees digitized on a lattice in the same way as the fracture pattern, using values of R_L in the range $(2^{1/2}, 2)$ and branching angles θ taking values of 0, $\pi/6$, $\pi/3$, $\pi/2$, $2\pi/3$ and π. When these trees were analysed using the mass–shell method, the dependence $\Delta M \sim e^{cR}$ was observed as was the case for the real fracture pattern. The slope, c, of the plot of $\log(\Delta M)$ versus R increased when R_L increased from $2^{1/2}$ to 2, but was much more sensitive to the branching angle, θ. This exponential increase of shell mass with radius is not that expected in the case of uniform fractals, for which a power-law dependence is found. Thus fractal trees do not exhibit simple "fractal" behaviour when analysed using the mass–shell method. The case $\theta = \pi$ and $R_L = 2^{1/2}$ is a special case for which a two-dimensional space-filling structure having $D = 2$ is expected [14, 33]. In this case we observe that $c = 0$ using the mass–shell method, i.e. no exponential dependence of shell mass with R. Instead a slower power-law dependence of mass versus R is obtained.

When the box-counting method was applied to the fractal trees having $R_B = 2$, the mass $M(k)$ covered by boxes of the iteration size k showed a k dependence similar to that observed for the fracture patterns. There were two regions of the plot. For small values of k, $D \sim 1$ and for values of k greater than the crossover k_{cr}, the fractal dimension obtained numerically depended mainly on R_L and not upon the branching angle, as expected [14]. For a particular value of R_L and $\theta > \theta_{cr}$ (i.e. for values of θ for which a tree structure rather than a closed loop structure is obtained), values of the fractal dimension, D, within our error bars (± 0.1) were obtained. The values obtained at θ_{cr} for each R_L are listed in Table II and are compared with the values of D calculated using Equation 7.

The error bars for D obtained by the box-counting method are ± 0.1. The corresponding values of the fractal dimension exponents obtained by the box-counting method and using Equation 7 are comparable. In the case $R_L = 2^{1/2}$ and $\theta = \pi$, a space-filling structure with $D = 2$ is expected, but we obtained a somewhat lower value of $D = 1.95$. For $R_L = 2$ the

TABLE II Fractal dimension exponents obtained for different R_L values using the box-counting method and relation $D = \ln 2/\ln (R_L)$

R_L	D		θ_{cr}
	Box-counting	$\ln 2/\ln (R_L)$	
2	1.0	1.0	0
1.8	1.3	1.2	54
1.5	1.65	1.7	152
$2^{1/2}$	1.95	2.0	180

expected value of D is 1, and we obtained that value at the critical angle $\theta_{cr} = 0$ and larger values for $\theta > \theta_{cr}$. The differences in D obtained from Equation 7 and from the box-counting method are probably due to the finite number of generations used to represent fractal trees as well as to lattice discretization of the problem. Equation 7 is valid in the asymptotic scaling region, corresponding to a large number of generations, while in our analysis only 12 generations were used. We have thus investigated the effect of increasing the number of generations on the value of D obtained by the box-counting method to determine whether this value of D approaches the calculated value of D (Equation 7). In order to observe the effect of increasing number of generations, it is necessary to increase resolution as well.

Increasing resolution, which was determined by the size of the largest branch I_0 from $I_0 = 100$ to 500 for a fixed number (13) of generations and with the fixed parameters $R_L = 2^{1/2}$, $R_B = 2$ and $\theta = \pi$, shifted k_{cr} to larger values of k. The value of D in the region $k > k_{cr}$ was slightly increased in the range (1.8–2) implying that for high enough resolution and large enough trees the expected value $D = 2$ would be approached. Then, at a fixed resolution of $I_0 = 500$, the number of generations was increased from 5 to 12, using the same parameters: $R_L = 2^{1/2}$, $R_B = 2$ and $\theta = \pi$. With increasing number of generations, the slope of the log $M(k)$ versus log k plot at large k (larger length scales) was not changed, but the slope at intermediate and small values of k (shorter length scales) increased and the crossover value of k, k_{cr} was shifted to smaller k.

The effect of different number of generations and resolution is shown in Fig. 11, where the data are plotted using a trial value D_{tr} of the fractal dimension exponent on the log–log plot of the scaled variables $y = M(k)2^{(k-1)D_{tr}}$ and $x = 2^{k-1}/[I_0/R_L^g]$. This plot presents a crossover function [11, 12] on which a data collapse for different values of g and k can be observed. The crossover at which the scaling behaviour changes occurs at $x = 1$, giving $k_{cr} = [\log(2I_0) - g \log(R_L)]/\log 2$. This is in agreement with the observation that the crossover value k_{cr}, decreases with the number of generations, g, and increases with resolution, I_0. A plot of y versus x should have two regions separated by $x = 1$. For values of $x < 1$, the slope is $D_{tr} - 1$ and for $x > 1$ (fractal regime) the slope is $D_{tr} - D$. The latter has zero slope for the best choice of D_{tr}, which in our case is $D_{tr} = 1.9$, as shown in Fig. 11. The effect of increasing number of generations on this plot was to make the flat region longer (i.e. to larger values of x) before finite size effects, which show up as an upward shift of y at large x, occur. The slope of the crossover function for the data at small x (or k) gives $D = 1$ as expected.

The discretization (lattice approximation) effect on the fractal dimension of exact trees obtained by box-counting method might also be important. The functional form of $D = \log 2/\log(R_L)$ is steeper for lower values of R_L and is thus sensitive to small changes in R_L for the smallest value of R_L we considered, namely for $R_L = 2^{1/2}$. Here, the effect of discretization might be most pronounced. We examined several effects of

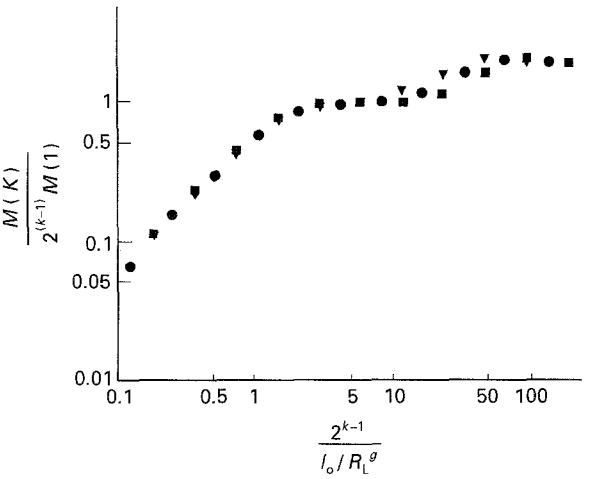

Figure 11 Log–log plot of scaled mass $M(k)/M(1)2^{k-1}$ versus scaled k: $2^{k-1}/[l_0/R_L^g]$ where l_0 is the length of the largest branch of the tree, g is the number of generations and $k_{cr} = \log(2I_0) - g \log(R_L)$ for $k/[I_0/R_L^g] = 1$. g = (■) 11, (●) 10, (▼) 9.

discretization in the case of trees with $R_L = 2^{1/2}$, $\theta = \pi$, including rotations of trees and shifts of the origin [39], and observed a slight change of the fractal dimension D in the range 1.85–2. However, these effects should be less important with increasing resolution.

We have also considered a modified version of exact trees having $R_B = 2$ and R_L fixed (= 1.8) and investigated the effect of varying the branching angle, θ, with generation number, i, on the values of fractal dimension, D, obtained by the box-counting method. We assumed a power-law dependence of θ_i, i.e. $\theta_i \sim \theta - (g + 1 - i)^{-x}$, where g is the size of the tree. For x in the range $(0, 1)$, there was only a slight change of fractal dimension from $D = 1.32$ (for $x = 0$) to $D = 1.36$ (for $x = 1$). Because we did not observe much effect on the fractal dimension when the branching angle, θ_i, of the tree structure was varied, it is not surprising that there was little effect on D when the value of θ was varied with generation number.

We note that a better comparison between the experimental fracture patterns and the exact tree model might be achieved by considering an ensemble of trees having the same R_L and θ values but different sizes (i.e. different number of generations). It can be shown that a superposition of individual trees of different sizes will broaden the crossover region but not affect the fractal scaling behaviour at large k.

4. Discussion

The patterns we observe on the fracture surfaces of ethoxylated bisphenol-A dimethacrylate resins were almost identical in appearance to those observed by Robertson and co-workers [29–31] and others [4, 40]. We have analysed the patterns in the regions of the "steps" and "stacked lamellar texture" in which the branching pattern is formed as a series of "steps" and "welts" originating from the crack front propagating on different planes. The branched fracture pattern, shown in Fig. 2, was analysed using three different

ordering schemes for labelling its branches. It was found that for the Strahler and inverted Weibel ordering schemes, the number of branches, average branch lengths and branch angles of a particular order, depended exponentially on that order. When Weibel's ordering scheme based on generation number orders was applied, a power-law scaling behaviour of those quantities better described the behaviour. The difficulty in determining whether a branching structure obeys an exponential or a power-law scaling behaviour has been discussed by West [34] and Horsfield [41] for the case of the diameters of bronchial trees. These were first reported to exhibit an exponential dependence on the order, but a power-law dependence [34] was found after applying a more detailed analysis using increased number of generations. In addition, it was found that the labelling scheme influenced whether the data were better fit by a power-law or exponential dependence [41]. The ordering scheme which ordered branches in the direction of increasing generation number fit the data better using a power law, while the Horsfield scheme which inverted this order fit the data better using an exponential fit [41]. We similarly found that generational ordering (i.e. Weibel scheme) fit our data for number of branches, average branch lengths and angles best using a power-law dependence and that the inverted ordering schemes (i.e. Strahler's and inverted Weibel) gave better fits to an exponential dependence.

The above scaling relations describing properties (i.e. number of branches, mean branch lengths and branching angles) of the fracture pattern in terms of order imply that the fracture pattern is a statistically self-similar structure. However, unlike homogeneous fractals for which any portion of the pattern when magnified isotropically looks statistically self-similar to the original pattern, our fracture pattern looks strikingly more similar to Mandelbrot's fractal trees. These are described as non-uniform fractals having different fractal dimensions for the trunks and tips. In this case, it is only when the outer portion of the pattern is magnified isotropically that it will look statistically similar to the original pattern. In the case of homogeneous fractals, branches of all sizes are distributed uniformally over the entire pattern, whereas in the case of non-uniform fractals, the smaller branches occur preferentially further away from the origin. Although our fracture patterns are similar to fractal trees, they are different in that the segments are curved and also that the branching angles decrease in going from the roots to the tips. Nevertheless, the fractal analysis we performed on the fracture patterns and fractal trees gave similar results, indicating that the model of non-uniform fractals might be applicable to the experimental fracture patterns.

When the box-counting method was applied to both fractal trees and the fracture pattern, the resulting plot of log $M(k)$ versus k exhibited the same behaviour, namely that it could be separated into two linear regions. For values of $k < k_{cr}$, corresponding to higher resolution (i.e. smaller length scales), the slope of the plot gave for the fractal dimension, a value close to $D = 1$. This is expected because in the region of high resolution all the branches of the fracture pattern appear as linear objects. For $k > k_{cr}$ a higher value of the fractal dimension was observed indicating the onset of fractal behaviour of the branching pattern. For our fracture pattern a value of $D = 1.4$ was observed in this region of k. For the case of fractal trees, the fractal dimension in this region was found to depend on the length ratio, R_L, but not much on the value of the branching angle, and ranged between $D = 1$ and 2.

This behaviour is that expected for non-uniform fractals with $D = 1$ for the trunks and $D > 1$ for the tips. For a given k (or box size, ε) the interior region of the tree consists of those branches having lengths greater than ε and behaves as a linear structure having $D = 1$, while the exterior of the pattern has $D > 1$. The trunk, i.e. the longest branch in the interior of the pattern, has $D = 1$ for any resolution up to its size. When a DLA structure is grown numerically, the minimum branch size is usually a pixel size ($k_{cr} = 1$) and the region with $D = 1$ is not observed. However, for other uniform fractals, this crossover behaviour is also observed when the pixel size of the lattice is smaller than the smallest branches of the structure [42].

It is important to examine why the box-counting method when applied to both exact trees and the fracture pattern (both non-uniform fractals) gives the same fractal scaling behaviour in the region $k > k_{cr}$, as in the case of uniform fractals. It is clear that for our branching pattern, as well as for the fractal trees, branches of different sizes, starting with the smallest ones at the tips, are spatially distributed in shells of different radii. For example, the shortest branch segments are the tips which occur preferentially at the periphery (i.e. the arrest line) of the pattern, and are not distributed uniformly over the whole pattern as in the case of uniform fractals. The shell next to the tips contains branches of average size greater than the average size in the first shell and as the origin is approached, the average branch length increases. These restricted spatial distributions of branches of particular sizes cause the interior of the branching pattern to be empty in comparison with uniform fractals, e.g. DLA structures, for which branches of different sizes are distributed uniformally over the pattern. When the box-counting method is applied to either uniform or non-uniform fractals it eliminates those branches which are smaller than the particular box size by the same amount, whether or not they are distributed uniformly as in the case of uniform fractals, or in restricted regions of space as in the case of non-uniform fractals. Thus the box-counting method will provide the same kind of information for both uniform and non-uniform fractals.

The value of the fractal dimension $D = 1.4$ obtained by applying the box-counting method to our fracture pattern agrees with the value of D obtained from Equation 7, commonly used in describing branched structures, for the cases of both Strahler's and inverted Weibel's schemes. In the case of exact trees, we obtained good agreement for $R_L = 2^{1/2}$, 1.5, 1.8 and 2. This is perhaps expected, because Equation 7 is derived for fractal structures where N_i and L_i depend

exponentially on the order i. The exact trees were generated assuming this dependence and the Strahler and inverted Weibel (but not the Weibel) schemes exhibited this dependence for the fracture patterns. A greater discrepancy in some cases may be due to lattice effects or to the fact that we have not reached the asymptotic scaling region of fractal behaviour. In the case of DLA this same comparison indicated that $D = 1.6 \pm 0.1$ using Equation 7 and $D = 1.62 \pm 0.02$ or 1.67 ± 0.03 using the box-counting method [11, 12].

The mass–shell method for characterizing both the fracture pattern and the exact trees provides more useful information on how the mass of the pattern is spatially distributed in the radial direction. By applying this mass–shell method, we found that the mass of the pattern (i.e. the number of occupied pixels) grew exponentially with the radius in both cases. In the case of exact trees, the exponential increase of mass with radius depended on the branching angle (for given R_L and R_B). For the fracture patterns, there were additional factors which caused the density to increase even faster with R: (i) the branching angle decreased with generation number causing the branches to be closer together, and (ii) the curvature of the branches towards the radial direction permitted closer packing of the branches. The constrained spatial distribution of branches (e.g. the interior of the pattern is empty compared with the more numerous smaller branches densely distributed close to the periphery) causes the dense packing which results in the exponential increase of mass with R. This result is completely different than the case of ordinary fractal structures embedded in a Euclidean space of dimension d, for which the mass $M(R)$ inside the circle of radius R grows with a power-law behaviour, i.e. as $M(R) \sim R^D$. This exponential increase of mass $M(R)$ with R (i.e. that the slope of M versus R, which is D, increases with R) can be formally associated with the fact that in the case of these non-uniform fractals, D increases as we go away from the origin.

5. Conclusion

The application of scaling and fractal geometry to fractured ethoxylated bisphenol-A dimethacrylate resins has provided a quantitative description of the tree-like patterns observed on a portion of the fracture surfaces. It was found that for the Strahler and inverted Weibel ordering schemes the average number of branches and branch lengths depended exponentially on the order. The bifurcation, R_B, and length, R_L, ratios, describing the relationship between the average number and lengths of branches in successive orders, respectively, were found to be $R_B = 2.5$ and $R_L = 1.9$ in the case of the Strahler scheme and $R_B = 1.8$ and $R_L = 1.55$ for the inverted Weibel scheme. For the latter, the average branch angles also depended exponentially on the order, with $R_\alpha = 1.13$. For fractal branching structures in which the number and lengths of branches depend exponentially on the branch order, the fractal dimension, $D = \log(R_B)/\log(R_L)$. Using this relationship, $D = 1.43$ and 1.35 for the Strahler and inverted Weibel schemes, respectively, which agreed well with the value of $D = 1.4 \pm 0.1$ obtained when the box-counting method was used to obtain the fractal dimension. The branching structure of the fracture pattern, which has been previously observed in other fractured polymers, metallic glasses and crystals, resembled a fractal tree, which is an example of a deterministic, self-similar, non-uniform fractal. Because computer algorithms could generate fractal trees (with exponential scaling behaviour for the branches) with more generations than were observed experimentally, a comparison was made between the fractal dimension obtained from the topological characterization and that from the geometrical characterization of fractal trees. It was found that the value of D from $D = \log(R_B)/\log(R_L)$ agreed well with that obtained using box counting. However, the mass–shell method for both the fractal tree and the experimental pattern gave a mass of the pattern which grew exponentially with the radius, rather than the power-law dependence expected for a uniform fractals.

Acknowledgements

The authors thank Dr P. Meakin for helpful discussions and suggestions, Dr D. Silage for the use of the digitization equipment and software, and G. Cowperthwaithe, Esschem, for providing the materials. This investigation was supported in part by Research Grant MSS-9210713 from the National Science Foundation, Mechanics and Materials Program, and Research Grant DE09530 from the National Institute of Dental Research, Bethesda, MD 20892.

References

1. M. J. DOYLE, A. MARANCI, E. OROWAN FRS and S. T. STARK, *Proc. R. Soc. (Lond.)* **A329** (1972) 137.
2. E. H. ANDREWS, "Fracture in Polymers" (American Elsevier, New York, 1968).
3. A. J. KINLOCH and R. J. YOUNG, "Fracture Behaviour of Polymers" (Applied Science, London, New York, 1983).
4. H. H. KAUSCH, "Polymer Fracture", 2nd Edn (Springer, Berlin Heidelberg New York, 1987).
5. C. S. SMITH, *Rev. Mod. Phys.* (1964) 524.
6. F. SPAEPEN and D. TURNBULL, *Scripta Metall.* **8** (1974) 563.
7. R. E. HORTON, *Geol. Soc. Am. Bull.* **56** (1945) 275.
8. A. N. STRAHLER, *Trans. Am. Geophys. Union* **34** (1953) 345.
9. *Idem, ibid.* **38** (1957) 913.
10. E. R. WEIBEL, "Morphometry of the human lung" (Springer, Berlin, 1963).
11. E. L. HINRICHSEN, K. J. MALOY, J. FEDER and T. JOSSANG, *J. Phys. A* **22** (1989) L271.
12. J. FEDER, E. L. HINRICHSEN, K. MALOY and T. JOSSANG, *Phys. D* **38** (1989) 104.
13. P. OSSADNIK, *Phys. Rev. A* **45** (1992) 1058.
14. B. B. MANDELBROT, "The Fractal Geometry of Nature" (Freeman, San Francisco, 1982).
15. J. FEDER, "Fractals" (Plenum, New York, 1988).
16. T. VICSEK, "Fractal Growth Phenomena" (World Scientific, Singapore, 1989).
17. P. MEAKIN, *Science* **252** (1991) 226.
18. P. MEAKIN, G. LI, L. M. SANDER, E. LOUIS and F. GUINEA, *J. Phys. A* **22** (1989) 1393.
19. T. A. WITTEN and L. N. SANDER, *Phys. Rev. Lett.* **47** (1981) 1400.

20. P. MEAKIN, in "Phase Transitions and Critical Phenomena", edited by C. Domb and J. L. Lebowitz (Academic Press, New York, 1987) pp. 336–489.
21. K. J. MALOY, J. FEDER and T. JOSSANG, *Phys. Rev. Lett.* **55** (1985) 2688.
22. K. J. MALOY, F. BOGER, J. FEDER, T. JOSSANG and P. MEAKIN, *Phys. Rev. A* **36** (1987) 318.
23. H. A. LAROCHE, J. F. FERNANDEZ, M. OCTAVIO, A. G. LOESER and C. J. LOBB, *ibid.* **44** (1991) R6185.
24. E. BEN-JACOB and P. GARIK, *Phys. D* **38** (1989) 16, and references therein.
25. F. FAMILY and T. VICSEK, "Dynamics of Fractal Surfaces", (World Scientific, Singapore, 1991).
26. B. MANDELBROT, *Phys. Scripta* **32** (1985) 257.
27. F. GREY and J. K. KJEMS, *Phys. D* **38** (1989) 154.
28. W. S. SHIN, X. F. LI, B. SCHWARTZ, S. WUNDER and G. BARAN, *J. Dent. Mater.*, **9** (1993) 317.
29. R. E. ROBERTSON and V. E. MINDROIU, *J. Mater. Sci.* **20** (1985) 2801.
30. *Idem, Polym. Eng. Sci.* **27** (1987) 55.
31. T. Y. PAN, R. E. ROBERTSON and F. E. FILISKO, *J. Mater. Sci.* **24** (1989) 3635.
32. J. VANNIMENUS, in "Universalities in Condensed Matters", edited by R. Jullien, L. Peliti, R. Rammal and N. Boccara (Springer, Berlin, 1985).
33. N. MacDONALD, "Trees and Networks in Biological Models" (Wiley, New York, 1983).
34. B. WEST, "Fractal Physiology and Chaos in Medicine" (World Scientific, Singapore, 1990), and references therein.
35. F. CASERTA, H. E. STANLEY, W. D. ELDRED, G. DACCORD, R. E. HAUSMAN and J. NITTMANN, *Phys. Rev. Lett.* **64** (1990) 95.
36. F. FAMILY, B. R. MASTERS and D. E. PLATT, *Phys. D* **38** (1989) 98.
37. T. MATSUO, R. OKEDA, M. TAKAHASHI and M. FUNATA, *Forma 5* **19** (1990).
38. J. VANNIMENUS and X. G. VIENNOT, *J. Stat. Phys.* **54** (1989) 1529.
39. V. K. HORVATH and H. J. HERRMANN, *Chaos Solitons Fractals* **1** (1991) 395.
40. A. C. MOLONEY and H. H. KAUSCH, *J. Mater. Sci. Lett.* **4** (1985) 289.
41. K. HORSFIELD, *J. Appl. Physiol.* **68** (1990) 457.
42. D. G. TARBOTON, R. L. BRAS and I. RODIGUEZ-ITURBE, *Water Resources Res.* **24** (1988) 1317.

Received 24 May 1993
and accepted 25 November 1994